Pulse monitoring based on transverse SHG
in periodic and disordered media

Robert Fischer[a], Dragomir N. Neshev[a], Solomon M. Saltiel[a,c], Andrey A. Sukhorukov[a],
Wieslaw Krolikowski[b], Ady Arie[d], and Yuri S. Kivshar[a]

[a]Nonlinear Physics Center and Laser Physics Center, and
[b]Laser Physics Center and Laser Physics Center,
Research School of Physical Sciences and Engineering, Australian National University,
Canberra ACT 0200, Australia

[c]Dept. Quantum Electronics, Faculty of Physics,
Sofia University, 1164 - Sofia, Bulgaria

[d]School of Electrical Engineering, Faculty of Engineering,
Tel-Aviv University, Ramat Aviv, Tel-Aviv, Israel

ABSTRACT

We study the second-harmonic generation via transversely-matched interaction of two counter-propagating ultra-short pulses in $\chi^{(2)}$ photonic structures with either random ferroelectric domains or annular periodic poling. The profile of the transverse second-harmonic signal is given by the cross-correlation of the pulses and can be used to characterise the temporal structure of the pulses.

Keywords: transverse second-harmonic generation, disordered nonlinear material, pulse characterisation

1. INTRODUCTION

The spatial distribution of transverse second-harmonic (TSH) signals from two counter-propagating light pulses represents the correlation of these pulses – thus providing a very simple tool for characterising and monitoring ultra-short pulses. In contrast to the alignment critical and time consuming measurements with regular autocorrelators, this pulse characterisation technique only requires the recording of the emitted TSH light e.g. with a CCD camera. However, TSH generation either by a single or by two counter-propagating waves [1,2] has proven to be a very challenging nonlinear optical effect. It can not be observed in bulk nonlinear crystals due to the lack of phase matching. In order to fulfill the required phase-matching condition, often layered or periodically poled media is used to achieve so-called quasi phase-matching. The first successful experiments with TSH have been conducted in $1-2\,\mu m$ thick quantum wells waveguide structures.[1,2] Because of this thin-film geometry, the transverse emission of SH from the waveguide structures is frequently called the surface emitting SH generation.

In this work we show how the interaction of counter-propagating beams in nonlinear quadratic crystals such as SBN leads to TSH which can be used for convenient autocorrelation measurements of femtosecond pulses. On the other hand, TSH can also be achieved in periodically poled crystals such as Lithum Niobate or Lithium Tantalate. Comparing two kinds of $\chi^{(2)}$ photonic materials, one with an annular periodic poling and one with a random ferroelectric domain structure, we study the physics of the TSH generation process and evaluate them for the use of pulse duration measurements.

2. TRANSVERSE PHASE MATCHING IN SBN

Naturally grown (unpoled) Strontium Barium Niobate (SBN) is known to quasi-phase-match any parametric process like for example second harmonic generation (SHG) or sum-frequency mixing (SFM) in an ultra-broad frequency range: without any crystal poling, the limitations of the bandwidth are mainly given by the transparency window of the crystal in the range of 0.4 - 6 μm.[3] This is of special importance for ultra-short pulses, for
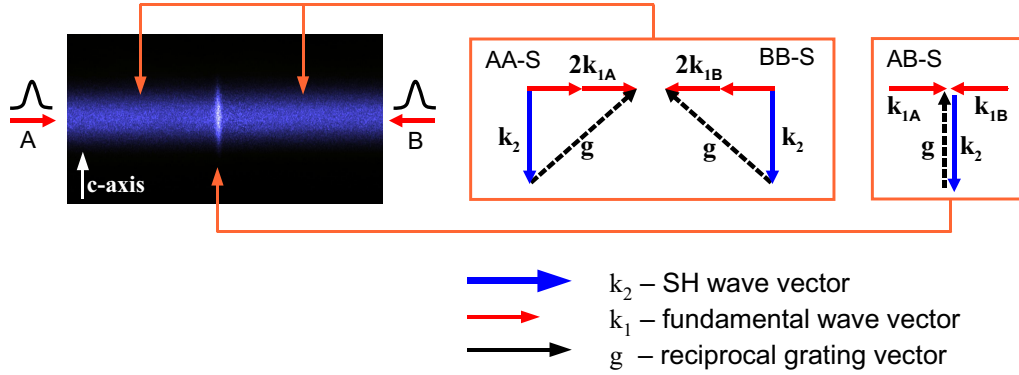
Figure 1. Transverse phase-matching of second-harmonic generation from two pulses counterpropagating perpendicular to the crystal z-axis ($k_1 \perp z$).

which the full spectrum is converted tuning-free with the same efficiency.[4] The disordered structure of antiparallel ferroelectric domains in this crystal provides a continuous set of grating vectors $\mathbf{g}$ to fulfil the phase-matching condition $\mathbf{k_2} = 2\mathbf{k_1} + \mathbf{g}$ not only for multiple frequencies simultaneously but also in all directions within a plane perpendicular to the crystal z-axis. The phase matching condition for two pulses with the same carrier frequency is depicted in Fig. 1, where it can clearly be seen that for the TSH of a single beam (AA-S and BB-S) and that of two counterpropagating pulses (AB-S) different phase-matching periods are required and therefore different domain sizes (d) in the crystal are involved. In practice, such sub-wavelength size domains are not available in the crystal,[5] thus the frequency conversion processes are phase-matched via higher-order QPM processes.

In our experiments, we use a femtosecond Ti:sapphire oscillator as source with pulse energies of 6 nJ, a repetition rate of 76 MHz, and tunability in the range of 700 to 900 nm. For the results presented in this work the laser was set to 850 nm. As shown in the schematic of the setup in Fig. 2, the laser beam is split into two arms of equal length before the two colinear counterpropagating pulses meet in a SBN crystal of 5 mm width. Each of the pulses generates a second harmonic trace in the crystal that is recorded by a CCD-camera mounted perpendicular to the beams and the crystal z-axis. The combined photo at the right side of figure 2 shows the camera view on the crystal where the top part of the picture is taken with background illumination to show the crystal dimensions (5 mm width) relative to the observed signal.

At the intersection of the two pulses they generate a clear peak on the SH background. In this particular configuration, when the two counter-propagating signals are identical, the generated normalised signal $I_{tot}(\tau)$ is given as $I_{tot}(\tau) = 1 + \frac{2}{R}G^{(2)}(\tau)$, where R is the ratio of the efficiencies of the SHG processes from the single and the couterpropagating pulses and $G^{(2)}(\tau) = \langle I(t)I(t+\tau)\rangle/\langle I^2(t)\rangle$ represents exactly the autocorrelation of the pulse. This experimental geometry results in a mapping of time (τ) into a space (longitudinal) coordinate (s) via the simple relation $\tau = s\, 2n_\omega/c$, where n_ω is the SBN refractive index dependent on the optical frequency,[6] and c is the speed of light in vacuum. Hence, the longitudinal distribution of the SH signal represents a time-dependent autocorrelation signal. We note that this is a single-shot technique, and it does not require any variable differential delay during the correlation recording. Measurements with an uncooled CCD-camera were done at power levels down to $0.26\,\mathrm{MW/cm^2}$, four orders of magnitude lower than those usually used with the comparable two-photon fluorescence (TPF) method .[7,8] The significantly lower power requirement is mainly due to the confinement of the emitted SH in a plane compared to the emission in the full solid angle from the TPF process.

The measurement accuracy is primarily limited by the imaging of the correlation trace onto a camera. For recording, we use an optical microscope at 4.5X magnification. To avoid an image distortion caused by the limited depth of field, the beams are focused in the crystal by cylindrical lenses ($f = 50\,\mathrm{mm}$), resulting in a beam width of $33\,\mu\mathrm{m}$ along the observation direction. For comparison, we also measured the pulse duration with a GRENOUILLE, as shown in Fig. 3(c,d). In Fig. 3(b) we overlay the SH autocorrelation trace (black dots)
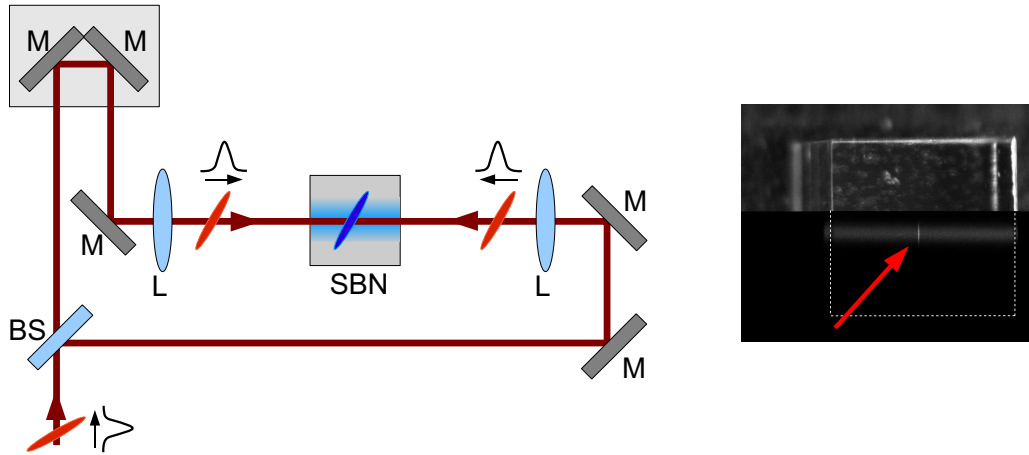
Figure 2. Experimental setup with BS - beam splitter, M - mirror, L - Lens. The combined photo on the right shows the camera perspective where top part is taken with background illumination for a comparison of the signal trace to the crystal width of 5 mm.
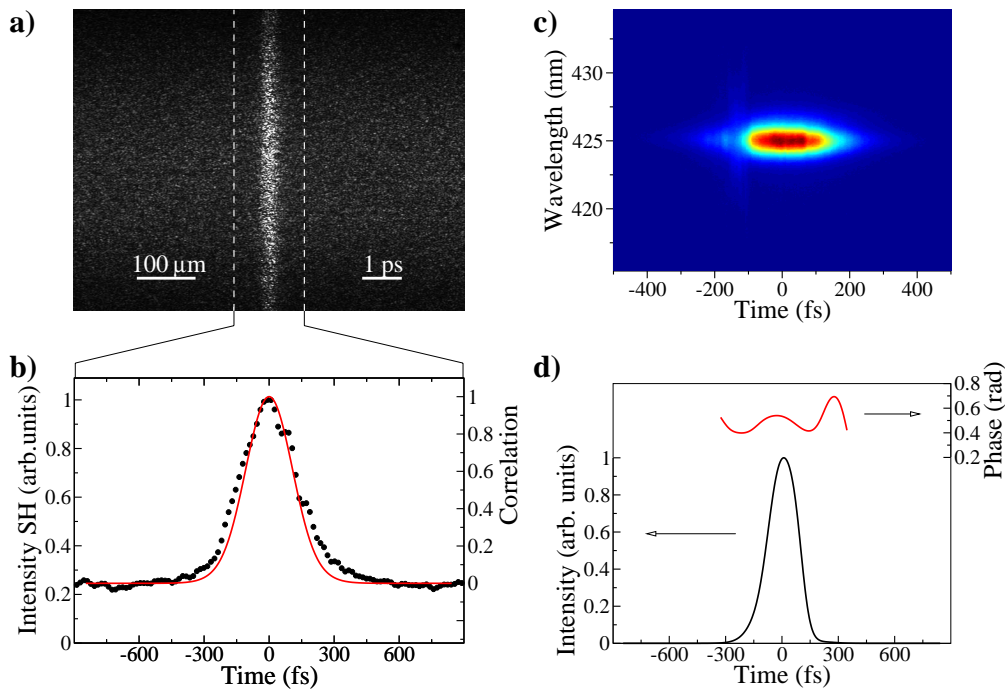
Figure 3. Comparison to FROG: (a) FROG trace, and (b) camera picture of transverse SH trace of the same pulse; (c) pulse shape and phase retrieved from FROG with $T_{FWHM} = 189$ fs; (d) black dots - SH profile from area marked in (b), solid line - autocorrelation calculated from FROG measurement.

with that obtained from the reference measurement taken with GRENOUILLE (red solid line). In a series of measurements we find the two methods to disagree no more than 10 %, including the dispersion of the 190 fs pulse in 2.5 mm of SBN, that accounted for approximately 4.5 % of the error. The effect of dispersion can be easily reduced by using shorter crystals.

Apart from the pulse duration measurements, the correlator in Fig. 2 can also be used to visualize unambiguously the tilt of the front of an optical pulse. Such a pulse front tilt (PFT) (which is typically caused by dispersive elements like prisms, gratings, or wedges) leads to an effective longer pulse duration and hence a lower
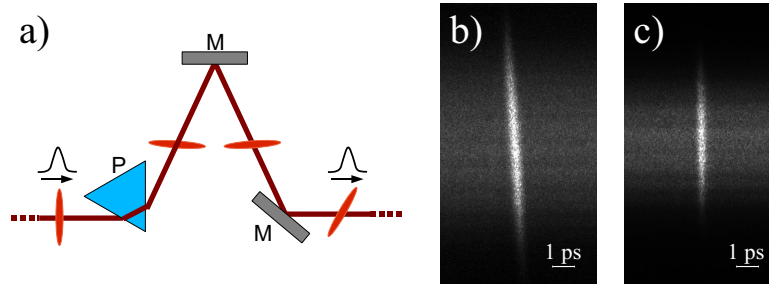
Figure 4. Visualizing pulse front tilt. (a) Schema of module to introduce pulse front tilt and autocorrelation (b) with and (c) without the module.
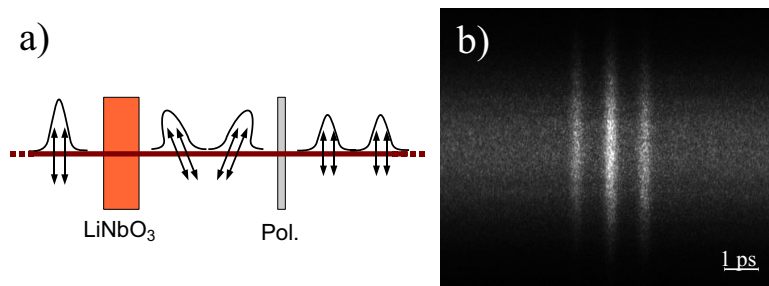
Figure 5. Visualizing complex pulse shapes and pulse trains. (a) A birefringent crystal is used to generate a pulse doublet. (b) The autocorrelation shows the delay of 989 fs between the pulses.

peak power in the focal plane of the beam. By placing a 60 degree (SF11 Schott glass) prism into the beam path [Fig. 4(a)], a PFT was introduced that can be clearly seen in the 4 degree tilt of the correlation trace [Fig. 4(b), compare with Fig. 4(c)].

The large time window of our technique ($1 \, \text{mm} \stackrel{\wedge}{=} 7 \, \text{ps}$) allows for monitoring more complex temporal structures consisting of multiple pulses. To demonstrate this feature, a pulse doublet is generated by passing the beam through a thin ($3.2 \, \text{mm}$) birefringent (lithium niobate) crystal followed by a polarizer, as depicted in Fig. 5(a). The ordinary polarized component of every pulse gets delayed roughly $1 \, \text{ps}$ with respect to its extraordinary counterpart. The polarizer combines these two components to a pulse doublet. The autocorrelation trace shown in Fig. 5(b) clearly resolves the two components of the doublet and allows for the delay between them to be precisely measured. For comparison, in the analogous experiment GRENOUILLE averages over the two pulses due to its narrow time window, hence the information about the double structure of the pulse event is completely lost.

In this autocorrelation scheme we make use of the biggest component of the $\chi^{(2)}$ tensor ($d_{zzz}^{(2)}$) for SBN, by directing the extraordinary polarised pulses perpendicular to the crystal's z-axis. However, if the absolute intensity of the SH signal can be compromised, background-free autocorrelation signals can be achieved by orientating the counter-propagating beams along the z-axis. The phase-matching conditions for this configuration are depicted in figure 6. The main difference to the situation depicted in figure 1 is the second-harmonic generation originating from the single pulses: The phase matching gratings under an angle to the propagation direction are not available in this configuration and so the SH is emitted in a cone at both sides of the crystal but not in transverse direction. Therefore, the SH background generated from these single pulses is not present for pulses propagating along the crystal z-axis. Only where the momentum of two photons from the counter-propagating pulses cancel out, transverse phase-matching is possible and SH is emitted [Fig. 6]. Thus the second-harmonic emission in transverse direction is restricted to the region and for the time of interaction of the two pulses, generating the background free auto-correlation shown in figure 7(left inset).
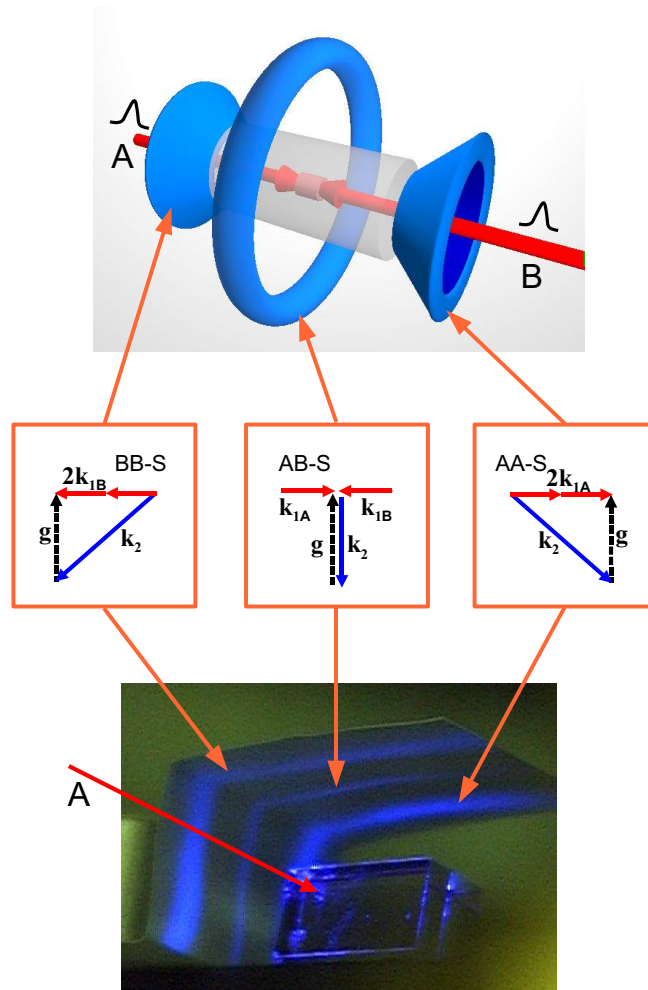
Figure 6. Generation of SH cones and toroidal wave for $k_\omega \parallel z$. The phase-matching condition for transverse second-harmonic is only fulfilled if the momentum of two counter propagating pulses cancel out. The second-harmonic wave from two fs-pulses then is emitted in form of a toroid.

3. TOROIDAL WAVES

A similar phase-matching situation can be a achieved in periodically poled Lithium Tantalate (PPLT), when the counterpropagating pulses are directed along the poling direction z. However, the two systems differ significantly in the properties of the phase-matching. We therefore compare the SHG in the disordered SBN structure with that of a an annular periodically poled Stoichiometric Lithium Tantalate (SLT) crystal.[9] The SLT sample is 0.49 mm thick and has an annular periodically poled structure in the x-y plane with the period of 7.5 μm.

As we already noted, no transverse SHG takes place in SBN for a single fundamental beam propagating along the z-axis. Instead, each pulse emits continuously a SH signal in the form of a cone,[4, 10] as shown schematically by the cones on the both side of the crystal in Fig. 6. These cones are clearly seen in the experiments with SBN as two strong outer lines as shown in Fig. 6(bottom). Analogous conical emission takes place in the annular
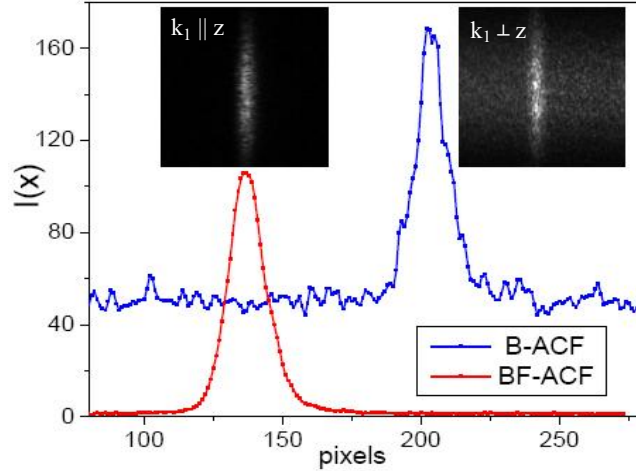
Figure 7. Camera pictures of transverse SH trace of the pulse and their autocorrelation function for $k_\omega \parallel z$(left) and $k_\omega \perp z$(right) geometries (taken at two different position of the delay line). One camera pixel corresponds to 15.7 fs. The ratio of SH intensities of the two curves does not reflect the real strength of the two processes.

periodically poled sample of SLT. The SH emission angle β is defined by relation $k_2.cos\beta = 2k_1$. The two cones are formed independently of the alignment of the two oppositely directed beams. Only when the two beams are exactly overlapped transverse SH wave is radiated. Since in that case the momenta of the two counter-propagating photons cancel out, transverse phase-matching can be achieved due to the reciprocal grating vector provided by the nonlinearity modulation. This can be seen clearly from the phase-matching diagram shown in the inset of Fig. 6(middle). The dashed arrow represents the effective reciprocal lattice vectors **g** while the solid red and the blue arrows denote the fundamental $\mathbf{k}_\omega$ and SH $\mathbf{k}_{2\omega}$ wave-vectors, respectively. Due to this phase-matching restrictions the SH is emitted only from the region of pulse overlap and only for the duration of the pulse interaction. It is exactly this spatiotemporal overlap that allows for the emission of a *spatiotemporal wave of a toroidal shape* [illustrated by the central ring in Fig. 6(top)]. The width and intensity profile of this wave along z direction is determined solely by the temporal correlation of the fundamental pulses, while the width and intensity profile in the transverse (x-y) direction (propagation direction of the toroidal wave) depends on pulse length and the fundamental beams spatial profiles.

Since for a beam propagating along the crystal z-axis the SHG process can not make use of the largest comonent d_{333} of the $\chi^{(2)}$ tensor, we amplify the pulses for the experiment in this configuration with a regenerative Ti:Sapphire amplifier operating at a wavelength of 830 nm. The system delivers linearly polarized 165 fs long pulses of energy up to 3 μJ at a repetition rate of 250 kHz. The beam with a Gaussian spatial profile is split in a polarizing beam splitter and directed from both sides to a quadratic nonlinear medium such that the same pulses meet roughly in the center of the sample. A set of $\lambda/2$ plates allows to control the relative powers of both beams and their polarizations. The average beam power before the beam-splitter is $\sim$ 340 mW. The two beams are loosely focused in the sample to 160 μm waist. All facets of both samples are polished and the emitted SH signal is recorded by a CCD camera.

The first-order transverse SHG phase-matching requires very fine grating periods. For the SLT sample, the necessary period is 183 nm for a 830 nm fundamental wave. As the grating period of our SLT sample is 7.5 μm the observed TSHG is thus due to a 41-st order phase-matching which, to the best of our knowledge, is the highest QPM order in crystals reported so far.[11] Naturally, such a high-order process results in a very low efficiency. The quadratic dependence of the SH signal on the power of the fundamental wave is verified by measuring the SH intensity in a particular single direction. To obtain angularly symmetric TSHG, it is essential to focus both counter-propagating beams exactly at the center of the annular domain structure. In contrast, the TSHG in SBN does not depend critically on alignment since the phase-matching conditions are the same everywhere in the crystal. Furthermore, since the average domain size is approximately 2.5 μm, the phase matching order is ca. 14 resulting in higher generation efficiency.
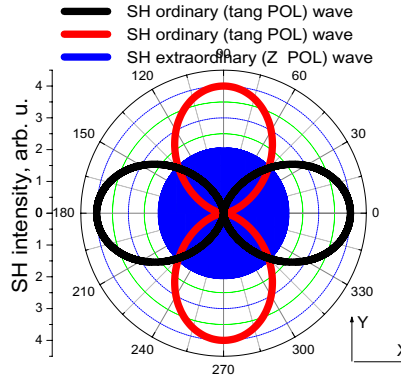
Figure 8. Theoretically determined emission diagram in polar coordinates $(I2, \alpha)$ of the toroidal wave. Dashed line: phase matched OO-E interactions (in SLT and SBN); Dashed-doted and solid lines: OO-O interaction (in SLT only) for both input polarizations either parallel along x, or y (dash-dotted) or mutually perpendicular along to x and y directions (solid).

As different nonzero values of the $\chi^{(2)}$ components are involved in transverse SHG in SBN and SLT, the emission diagrams for both structures are also different. The calculated emission diagrams in polar coordinates (I_2, α) where α is the emission (observation) angle for the ordinary and extraordinary polarized toroidal waves are shown in Fig. 8. In the case of the OO-E interaction (ordinary polarized fundamental beams and extraordinary polarized SH) the relevant nonzero $\chi^{(2)}$ components in both crystals are d_{zxx} and $d_{zyy} = d_{zxx}$. The generated toroidal wave is polarized along the z-axis of the crystal and its intensity is constant for all emission directions in the x-y plane. However, the SH intensity depends critically on the polarization of the fundamental waves $I_{2,ex} \propto [d_{zyy}I_1 \cos(\gamma_1 - \gamma_2)]^2$, where γ_1, γ_2 denote the angles of input polarizations for both the beams measured counterclockwise with respect to the x-axis. In contrast to SBN where the OO-O interaction is impossible, in SLT the relevant $\chi^{(2)}$ components d_{yyy} and $d_{yxx} = -d_{yyy}$ allow for the generation of an ordinary SH wave polarized in the x-y plane with its intensity varying with the emission angle α and input polarization directions as $I_{2,o} \propto [d_{yyy}I_1 \sin(\gamma_1 + \gamma_2 - \alpha)]^2$.

Since our samples are not cylindrical, it was not possible to measure accurately the angular variations of the intensity of SH. Instead, we measured the SH intensity and polarization properties of the emitted wave along the x- and y-axis of the crystal vs. the polarization angles γ_1, γ_2. The experimental results for both SBN and SLT crystals are shown in Fig. 9 together with the theoretical curves. The graphs in Fig. 9(a) show the measured SH signal emitted in the SBN crystal (points) as a function of γ_1 for few values of γ_2. The agreement with the expression for $I_{2,e}$ (solid lines) of the OO-E interaction is excellent. For the SLT crystal the polarization dependencies are more complicated due to the simultaneous contribution of both OO-O and OO-E interactions [see Figs. 9(b,c)]. Plots in Fig. 9(b) show the dependence of the total intensity of the SH signal on the polarization of the fundamental beams. On the other hand, in the case displayed in graph Fig. 9(c) both fundamental beams were either parallel (X direction - circles) or orthogonally (X and Y directions - squares) polarized. The SH signal is then measured as a function of the angular position (δ) of the analyzer mounted in front of the CCD camera. For parallel polarized fundamental beams, both OO-E and OO-O processes contribute to the SH signal. Hence the recorded signal contains both ordinary and extraordinary components and never vanishes. For orthogonally polarized input beams, the SH wave is ordinary polarized (due to OE-O process) and the recorded SH signal vanishes at the angles $\delta = (-\pi/2, \pi/2, 3\pi/2)$.

A quantitative analysis of the experimental data indicates that the contribution of the OO-E process governed by the d_{zyy} component is stronger than that of the OO-O process governed by the d_{yyy} component. This does not agree with the value $d_{zyy}/d_{yyy} = 0.59$ reported earlier.[12] This contradiction can be explained by the fact that OO-E process is closer to the exact phase matching condition than the OO-O process. We also note that for the SBN sample the SH generation process is practically independent of the fundamental wavelength within
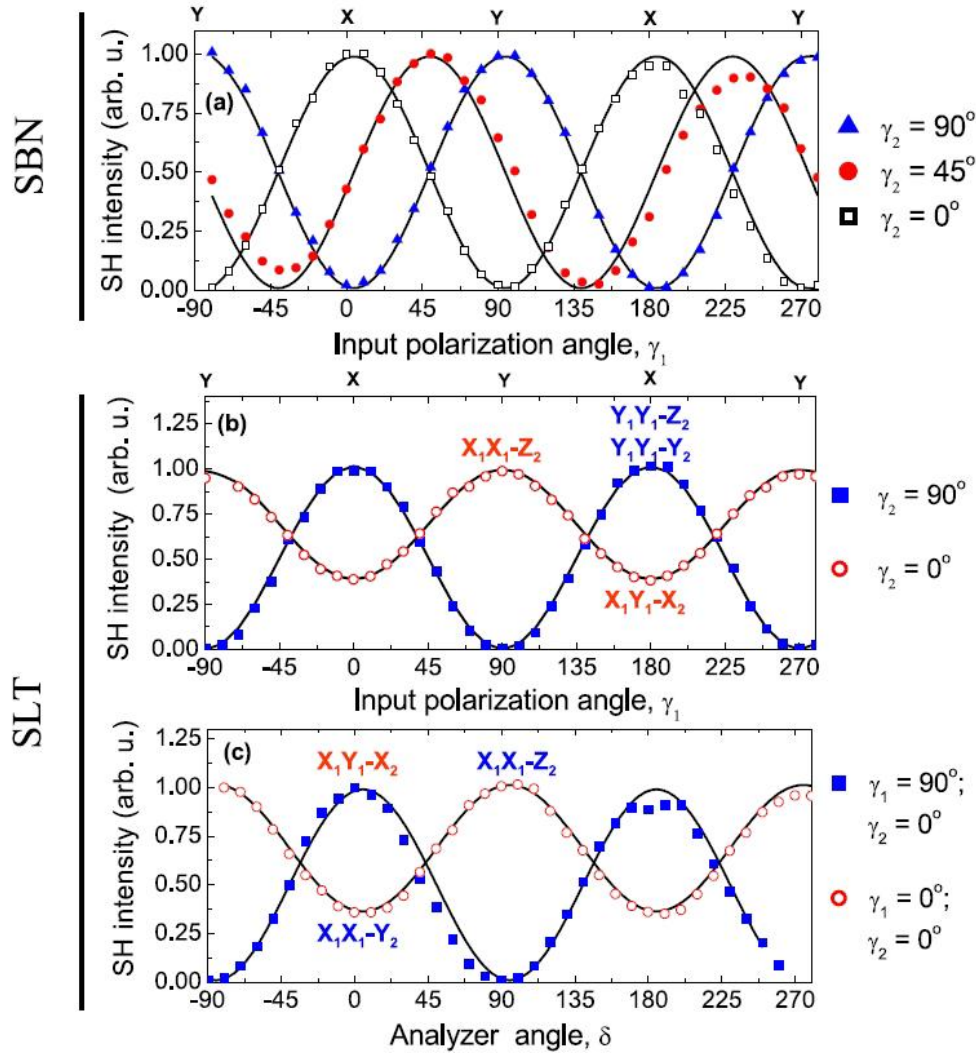
Figure 9. Polarization characteristics of SHG in (a) SBN and (b-c) SLT: (a) Intensity of the SH signal as a function of the input polarization angle γ_1, for three values of γ_2; (b) total SH signal in the SLT sample as a function of the input polarization angle γ_1 for indicated values of γ_2; (c) Intensity of the SH signal generated in the SLT sample as a function of the angle (δ) of an analyzer mounted in front of the CCD camera. In all plots solid lines represent the theoretical results.

a broad frequency range.

Due to the transverse geometry of the parametric interaction, the transverse SHG signal effectively translates the time coordinate into the space coordinate such that the width of the toroidal wave in the direction of the z-axis is exactly the autocorrelation function of the interacting pulses.[1, 13, 14] From calibrated experimental photo similar to one in figure 7(left inset) we measured the thickness of the toroid wave in SLT crystal to be 34 μm, that corresponds to 160 fs assuming secant hyperbolic temporal shape. Since the beam size is much bigger than the spatial extent of the pulse, the thickness of the toroidal waves in propagation direction outside the sample is determined by the beam size and is about 370 μm

In conclusion, we studied application of second harmonic process in quadratic nonlinear media for ultra-short pulse monitoring. We demonstrated an efficient and simple autocorrelation technique utilizing the counter-propagating transversely matched parametric process in crystals with either random or radially periodic ferro-electric domain distribution. We showed that this method allows to characterize basic properties of the short

pulses including width and front tilt. In addition, we showed that second harmonic formed in this process has a form of toroidal waves. By utilizing crystallographic properties of the nonlinear crystal this toroidal wave can be used to realize a background-free single short-pulse autocorrelator.

REFERENCES

1. N. D. Whitbread, J. A. R. Williams, J. S. Roberts, I. Bennion, and P. N. Robson, Opt. Lett. **19**, 2089 (1994).
2. A. Otomo, G. I. Stegeman, M. C. Flipse, M. B. J. Diemeer, W. H. G. Horsthuis, and G. R. Mohlmann, J. Opt. Soc. Am. B **15**, 7759-772 (1998).
3. M. Horowitz, A. Bekker, and B. Fischer, Appl. Phys. Lett. **62**, 2619 (1993).
4. R. Fischer, S. M. Saltiel, D. N. Neshev, W. Krolikowski, and Yu. S. Kivshar, Appl. Phys. Lett. **89**, 191105 (2006).
5. J. J. Romero, C. Aragó, J. A. Gonzalo, D. Jaque, and J. García Solé, J. Appl. Phys. **93**, 3111 (2003).
6. Th. Woike, Phys. Status Solidi A **186**, R13 (2001).
7. D. J. Bradley and G. H. C. New, Proceedings of the IEEE **62**, 313 (1974).
8. J. A. Giordmaine, P. M. Rentzepis, S. L. Shapiro, and K. W. Wecht, Appl. Phys. Lett. **11**, 216 (1967).
9. D. Kasimov *et al.*, Opt. Express **14**, 9371 (2006).
10. A. R. Tunyagi, M. Ulex, and K. Betzler, "Noncollinear optical frequency doubling in strontium barium niobate," Phys. Rev. Lett. **90**, 243901 (2003).
11. X. Gu, R. Y. Korotkov, Y. J. Ding, J. U. Kang, and J. B. Khurgin, "Backward second-harmonic generation in periodically poled lithium niobate," J. Opt. Soc. Am. B **15**, 1561-1566 (1998)
12. F. Charra and G.G. Gurzadyan, In: *Nonlinear Dielectric Susceptibilities*, ed. D.F. Nelson (Springer, Berlin, 2000).
13. R. Normandin, R. L. Williams, and F. Chatenoud, Electr. Lett. **26**, 2088 (1990).
14. R. Fischer, D. N. Neshev, S. M. Saltiel, A. A. Sukhorukov, W. Krolikowski, and Yu. S. Kivshar, Appl. Phys. Lett. **91**, 031104 (2007).